Lab on a Chip

PAPER

View Article Online
View Journal | View Issue

Cite this: *Lab Chip*, 2023, **23**, 4265

Magnetofluid-integrated biosensors based on DNase-dead Cas12a for visual point-of-care testing of HIV-1 by an up and down chip†

Di Huang,[ab] Yekai Zhao,[ab] Mengjun Fang,[ab] Peijie Shen,[ab] Hu Xu,[ab] Yichen He,[ab] Shengfu Chen,[ac] Zhenjun Si[d] and Zhinan Xu *[ab]

Received 25th June 2023,
Accepted 8th September 2023

DOI: 10.1039/d3lc00558e

rsc.li/loc

The CRISPR Cas system, as a novel nucleic acid detection tool, is often hindered by cumbersome experimental procedures, complicated reagent transfer processes, and associated aerosol pollution risks. In this study, an integrated nucleic acid detection platform named "up and down chip" was developed, which combined RT-RAA technology for nucleic acid amplification, DNase-dead Cas12a-modified magnetic beads for specific recognition of target nucleic acid, and HRP–TMB chromogenic reaction for signal output in different chambers of a single microfluidic chip. The magnetic beads were migrated in an up-and-down manner between different chambers through magnetic driving, achieving a "sample-in, result-out" detection mode. By introducing a homemade heating box for temperature control during the reaction and using the naked eye or a smartphone APP for color-based signal reading, no professional or precise instruments were required in this platform. Using this platform, highly sensitive detection of the HIV-1 genome as low as 250 copies (CPs) per mL was achieved within 100 min while maintaining good detection performance against common variants as well as excellent specificity and anti-interference ability. In addition, compared with qRT-PCR, it also exhibited good accuracy for 56 spiked plasma samples, indicating its promising potential for clinical application.

Introduction

Highly sensitive and specific nucleic acid detection is crucial for *in vitro* diagnosis of pathogenic microorganisms.[1,2] In recent years, the advancement of clustered regularly interspaced short palindromic repeat (CRISPR) technology has innovated the field of nucleic acid detection because it could sensitively discriminate single-nucleotide polymorphisms and possess outstanding signal amplification capacity.[3,4] For example, Cas12 is a type V CRISPR-associated protein which can precisely recognize the target DNA fragment and trigger a conformational change under the guidance of CRISPR RNA (crRNA), thereby sequentially activating its *cis*- and *trans*-cleavage activities.[5,6] Based on this principle, a range of novel nucleic acid detection technologies have been developed. The most representative DETECTR platform used a fluorescent single-stranded DNA (ssDNA) probe as the substrate for *trans*-cleavage so the concentration of target DNA could be transduced into a fluorescence signal, and thus the high-sensitivity genotyping detection of human papilloma virus was enabled with the aid of a fluorometer.[7]

To enhance the practicality of the CRISPR Cas12a system and make it amenable to point-of-care (POC) testing for nucleic acid, our group has designed various biosensors to transduce the detection targets into easily readable signals such as color,[8] distance,[9] and glucose,[10] which are easily distinguished by the naked eye or portable devices. Although these systems have made substantial improvements in portability and eliminated the dependence on large instruments, they still required multiple reaction processes, including nucleic acid amplification, target recognition by Cas effectors, signal amplification and transduction by CRISPR-based biosensors, and final data readout by corresponding devices.[11,12] Besides the cumbersome processes, this sectional detection mode may also engender unanticipated problems, especially aerosol contamination during the transfer of nucleic acid amplification products, which could obviously raise false positives and thus compromise the accuracy of testing results.[13–15]

[a] *Key Laboratory of Biomass Chemical Engineering of Ministry of Education, College of Chemical and Biological Engineering, Zhejiang University, Hangzhou 310027, China. E-mail: znxu@zju.edu.cn*
[b] *Institute of Biological Engineering, College of Chemical and Biological Engineering, Zhejiang University, Hangzhou 310027, China*
[c] *Institute of Pharmaceutical Engineering, College of Chemical and Biological Engineering, Zhejiang University, Hangzhou 310027, China*
[d] *Hangzhou FasTech Biotechnology Company Limited, Hangzhou 310005, China*
† Electronic supplementary information (ESI) available. See DOI: https://doi.org/10.1039/d3lc00558e

To simplify the above experimental operations without weakening detection performance, these multiple steps could be integrated into a closed and controllable space. In the past two decades, microfluidic technology has made significant contributions to improvements of various detection systems, particularly in integration and automation.[16,17] As the core concepts of this technology, interferences between multiple reaction systems could be prevented by the utilization of physical separation, while substance exchange within different chambers could be enabled through several fluid driving forces,[18] such as capillary force,[19] centrifugal force,[20] and magnetic force.[21]

Herein, an integrated POC testing system combining a CRISPR Cas12a-based biosensor and microfluidic technology was developed to address the aforementioned challenges. By using modified primers, the target RNA was converted into 5′ end biotin-labeled dsDNA through reverse-transcription recombinase-aided amplification (RT-RAA). Triggered by crRNA, DNase-dead Cas12a (dCas12a)-modified magnetic beads (MBs) could firmly capture target dsDNA and then bind to streptavidin-modified horseradish peroxidase (HRP) through affinity. Using a principle similar to that of enzyme-linked immunosorbent assay (ELISA),[22] the formed sandwich structure on the surface of MBs could efficiently catalyze the oxidation of 3,3′,5,5′-tetramethylbenzidine (TMB), so the resulting color change was directly recognized by the naked eye. Based on this scheme, multiple processes including nucleic acid amplification, target capture, affinity binding, MB washing, and color reaction were integrated into different chambers of a microfluidic chip and sealed with a unified oil-phase chamber to avoid interference. With the help of a magnet, the shuttle of MBs between the oil and the water phases enabled the substance exchanges in different chambers, and the final signal output was completed in the last chamber. Due to the movement of MBs in different chambers, this platform was named the "up and down chip". Moreover, the depth of shade in the color reaction chamber was converted to different RGB values by using a color recognizer application (app) developed for smartphones, and the corresponding luminance values were calculated using an empirical formula.[23–25] In this way, further signal transduction was achieved to improve detection sensitivity and made it possible to semiquantitatively/qualitatively detect target nucleic acid fragments without professional equipment. Subsequently, human immunodeficiency virus-1 (HIV-1) was applied as a model target for practical evaluation of this detection system and compared with the existing HIV-1 detection methods such as the "gold standard" quantitative reverse-transcription polymerase chain reaction (qRT-PCR). The results showed that our up and down chip could be read with the naked eye or a smartphone and achieved highly sensitive and specific detection without the requirement of large instruments. The entire detection process was integrated within a single chip, ensuring good safety and clinical application potential, which was practically significant for assessing viral load to improve patient survival rates.

Experimental methods

Materials and methods

HIV-1 pseudovirus, primers, probes, and other oligonucleotides used in this article (Table S1†) were ordered from TsingKe Biological Technology Co., Ltd. (Hangzhou, China). Streptavidin-modified HRP (HRP-SA) and nonfat powdered milk were purchased from Sangon Biotech Co., Ltd. (Shanghai, China). Soluble TMB substrate solution was bought from Tiangen Biotech Co., Ltd. (Beijing, China). Light mineral oil was bought from Sigma-Aldrich Co., Ltd. (St. Louis, USA). Ni-charged magnetic beads (MBs) were purchased from GenScript Co., Ltd. (Nanjing, China). Other chemical reagents were all analytical grade and purchased from Sinopharm Chemical Reagent Co., Ltd. (Shanghai, China). The laser engraving machine was purchased from ZhongGuang Dian Optoelectronic Technology Co., Ltd. (Liaocheng, China). Other consumables related to chip preparation were bought from YoungChip Co., Ltd. (Hangzhou, China). The metal ceramic heater (MCH) was purchased from Qianjin Special Ceramic Technology Co., Ltd. (Yixing, China).

Preparation of the dCas12a-modified beads

According to the literature, DNase-dead Cas12a used in this paper has a single amino acid mutation (E925A) compared to its wild-type form (*Lachnospiraceae* bacterium ND2006 Cas12a).[26] This dCas12a gene was constructed in pET28a as the expression vector. The *E. coli* BL21 (DE3) strain was selected for dCas12a expression, and protein purification followed a standard protocol as shown in the ESI.† The purified dCas12a was quantified by the bicinchoninic acid method and stored at −20 °C for further use.

To prepare dCas12a-modified MBs, after washing with 1× PBS buffer, MBs from 1 mL 25% slurry were mixed with 1 mL 400 nM His-tagged dCas12a and vertically incubated at room temperature for 20 min. After thorough washing with 1× PBS buffer, the dCas12a-MBs were mixed with 1 mL 2% nonfat milk solution overnight at 4 °C. Finally, the MBs were washed with 1× PBS buffer again and resuspended in storage buffer (10 mM Tris-HCl, 50 mM NaCl, 10 mM $MgCl_2$, 0.05% Tween 20, pH 7.9). The well-prepared dCas12a-modified MBs were stored at 4 °C for further use.

In vitro preparation of nucleic acids

In some optimization experiments, double-stranded DNA (dsDNA) was prepared as follows and used as the mimic target. Two complementary ssDNAs (Mimic target-F and -R in Table S1†) were incubated at 95 °C for 5 min and then annealed by cooling at a rate of 0.1 °C s^{-1} until reaching room temperature to prepare target dsDNA and stored at 4 °C for further use.

The crRNA of dCas12a was synthesized using an *in vitro* transcription kit (Thermo Fisher Scientific). The reaction system consisted of 2 μL transcription enzyme mixtures, 4 μL transcription buffer, 8 μL 10 μM NTPs, and 6 μL 5 μM dsDNA templates with a T7 promoter (Trans-F and -R). After reaction at 37 °C for 8 h, the products were purified using an RNA clean and concentrator kit for crRNA (Zymo Research) followed by quantification and storage at −80 °C for further use.

Preparation of the up and down chip

The up and down chip used in this paper was composed of four layers of polymethyl methacrylate (PMMA), whose sizes and structures were designed and optimized using AutoCAD. Due to the differences in thickness among the layers, the cutting power and speed used in the chip fabrication by the laser cutting machine were also different (shown in Table S3†). After washing with ddH_2O, soaking in 2% nonfat milk solution, and drying, the chip was assembled layer by layer using the adhesive force of optical double-sided tape. Finally, the well-prepared chips were stored in a desiccator until ready to be used.

Preparation of the homemade constant-temperature device

As shown in Fig. S8,† the device with dimensions of 80 mm × 80 mm × 38 mm mainly consists of three parts: a power module, a heating module, and a chip holder. The heating module employed a low-cost 40 mm × 40 mm MCH, which was an efficient, environmentally friendly, and safe heater. Two different power suppliers can be used to drive the MCH, which were placed in the bottom power module. The chip holder was used to place the up and down chip and separated it from the MCH by a 0.2 mm PMMA layer. The frames of these three parts were all assembled using PMMA and finally glued together using a PMMA-specific adhesive. During the characterization and optimization process, a handheld infrared detector was used to measure the temperature of the MCH and the chip chambers.

Sample pretreatment and extraction

In some optimization and comparison experiments, we employed a heat lysis method to process HIV-1 pseudovirus in the buffer. Specifically, 20 μL of the sample was incubated at 75 °C for 10 min to induce virus lysis and release RNA without any further extraction procedures. For the actual detection process, a commercial genomic extraction kit from BeaverBio was used. A total of 200 μL mimic samples (plasma, saliva, urine, or buffer) spiked with HIV-1 pseudovirus were extracted using MBs for approximately 20 min, followed by elution with 20 μL of RNase-free H_2O (10 min lysis, 5 min washing and purification, and 5 min elution). Finally, samples processed by the aforementioned two methods can be directly subjected to the subsequent RT-RAA reaction for detection. All samples were collected with the informed consent of healthy volunteers and all relevant tests were performed following the Guidelines for Ethical Management System of Zhejiang University, China.

Loading procedure of the up and down chip

Referring to Fig. 1A, 100 μL dCas12a-modified MBs stored with 2 μL 2 μM crRNA, 80 μL RT-RAA reaction solution (including 67 μL RT-RAA buffer to dissolve amplification enzyme mixtures from the kit bought from ZhongCe Bio-Technology, 8 μL of 5 μM primer mixtures, and 5 μL of amplification starter), 100 μL 250 nM HRP-SA solution, and 100 μL soluble TMB substrate solution were added in counterclockwise order to the circular chamber containing S_1, R_1, R_2, and R_3, respectively. The remaining three circular chambers (WB) were filled with washing buffer (1× PBS buffer with 0.75% Tween 20). Due to the surface tension, the aqueous solution quickly filled the circular chambers, and they remained isolated from each other because of the physical separation of the chip. Finally, the connected arc-shaped reservoir above the circular chambers was filled with light mineral oil. A practical demonstration is exhibited in Video S1.†

Detection procedure based on the up and down chip

The entire detection process was carried out by manipulating MBs using a columniform magnet (a basic operation mode can be found in Video S2†), allowing for rapid completion of the assay within 100 min including the sample pretreatment procedure described above. During this procedure, 20 μL of the extracted sample was added to the R_1 reaction chamber and gently mixed with the RT-RAA reaction solution by pipetting. Subsequently, the chip was placed in the homemade incubation device for 20 min to achieve isothermal nucleic acid amplification. After successive magnetic drives using a magnet above S_1 and below R_1, the MBs were migrated into R_1. Subsequently, the solution was mixed by rotating a magnet below R_1, allowing for the capture of target amplification products by dCas12a guided by crRNA. Following a 10 min incubation, the MBs were transferred using the same method and entered R_2 after a 2 min washing in the WB chamber. After 10 min of mixing in R_2, HRP-SA was fully bound to the biotin group present in the amplification products. The MBs were then sequentially transferred to two consecutive WB chambers, where they underwent a total of 4 min of washing before finally entering R_3 for chromogenic reaction. In the R_3 chamber, the intact "sandwich structure" formed on the surface of MBs with HRP catalyzed the oxidation of TMB to form a blue product for 20 min. To obtain a clearer image of the R_3 chamber, the MBs could be transferred to the previous WB chamber after the reaction. In this way, the detection signal based on color change could be read by the naked eye or a smartphone app.

Detection procedure based on RT-qPCR assays

The samples for qRT-PCR detection were extracted using the same procedure as the up and down chip-based method.

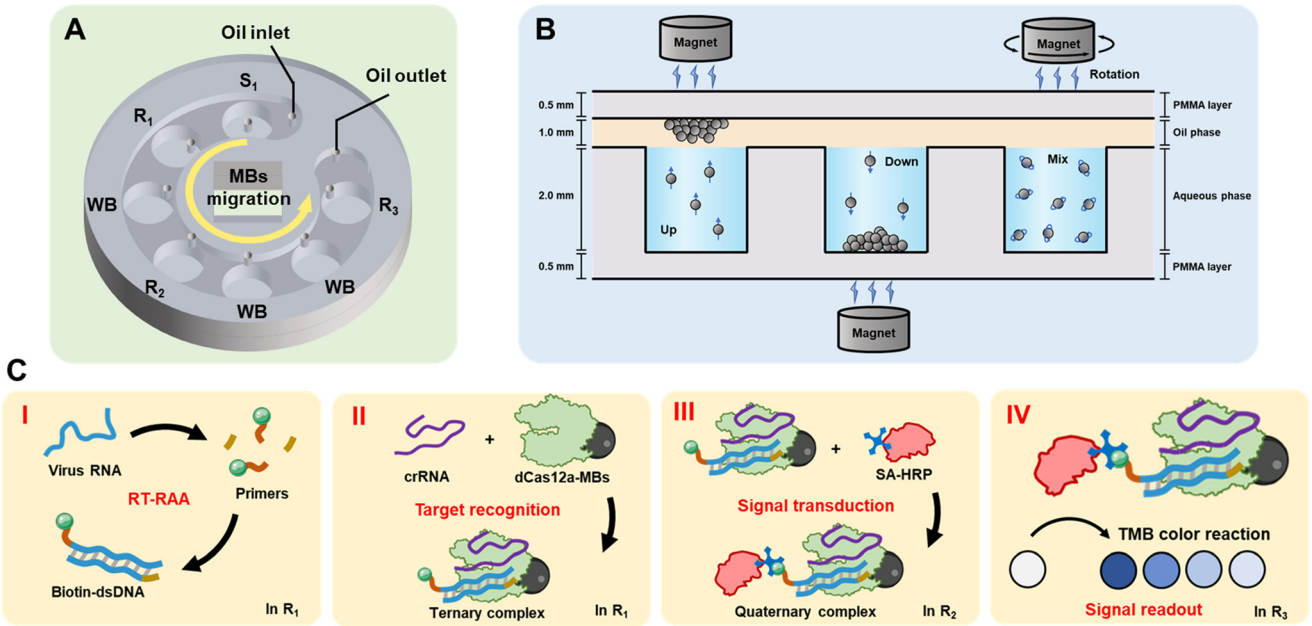

Fig. 1 Working principle of the up and down chip for HIV-1 detection. (A) Schematic diagram of the chip structure. (B) MB migration and mixing mode. (C) Principle of nucleic acid detection based on dCas12a in the up and down chip. (I) Reverse transcription and exponential amplification of target RNA through RT-RAA reaction. (II) Target recognition by dCas12a-modified beads. (III) Signal transduction through the capture of HRP-SA. (IV) Signal readout based on the color change reaction.

According to the manual of the qRT-PCR kit (Vazyme), the reaction system consisted of 1× Reaction Mix, 1× Rox Reference Dye, 0.2 μM primer mix, 0.1 μM Taqman probe, 10 μL samples, and RNase-free water added to make up the final volume to 20 μL. The standard qRT-PCR program included reverse transcription at 55 °C for 15 min, pre-denaturation at 95 °C for 30 s, 45 cycles of denaturation at 95 °C for 10 s and annealing/extension at 60 °C for 30 s. A fluorescence signal was acquired at the end of each cycle, and the thresholds were set at ten times the standard deviation recorded during cycles 3–15.

Results and discussion

Working principle of the up and down chip for HIV-1 detection

The design of the up and down chip (Fig. 1A) was aimed to integrate the diverse steps of traditional CRISPR Cas12a detection systems into a single device. It consisted of seven reservoirs for loading different reagents and a double-ended sealed arc structure for loading mineral oil, which blocked the contact between the reservoirs. Fig. 1B demonstrates that by magnetic control of the vertical and horizontal movements, MBs modified with dCas12a can be shuttled back and forth between the oil phase and the aqueous phase. Additionally, the rotation of the magnet facilitated the mixing between the reaction solutions and the MBs, allowing different reactions in distinct circular chambers. This magnetic manipulation provided a universal and effective way for conducting nucleic acid analysis based on MBs, which is similar to ELISA. As shown in Fig. 1C, the test HIV-1 sample was first injected into the R_1 chamber to allow reverse transcription and exponential amplification of targets through RT-RAA reaction. After that, the dCas12a-modified MBs were shuttled sequentially from S_1 through R_1, R_2, and several WB chambers to complete the binding of the target fragment, the capture of HRP-SA, and the washing process, respectively. Finally, the MBs with "sandwich structure" arrived at the R_3 chamber, so the HRP moiety in the MBs catalyzed the oxidation of TMB and enabled the detection of a target *via* the naked eye or smartphone app based on the color change reaction.

Establishment and optimization of the up and down chip

As illustrated in Fig. S1A–D,† the up and down chip consisted of four layers of PMMA, including a top layer with eight inlets and one outlet of 1.3 mm in diameter, a second layer with an arc-shaped oil phase chamber of inner and outer radii of 11 mm and 19 mm, respectively, a third layer with eight circular aqueous phase chambers of 8 mm in diameter, and a bottom layer as the support of the chip (each layer contained a 10 mm × 10 mm square for chip bonding, and the optimized thickness is presented in Fig. S1E–H†). The chip was prepared by layer-by-layer assembly with an appearance resembling ancient Chinese coins (Fig. S1I and J†).

To characterize the chip as shown in Fig. 2A (I), the green dye solution and colorless mineral oil were injected into the circular chambers and the arc-shaped chamber, respectively, and the two phases were well separated and stable. Since the migration of MBs was crucial for the reaction and the detection performance, the migration efficiency was optimized in the aspects of surfactant aqueous concentration and layer thickness by using

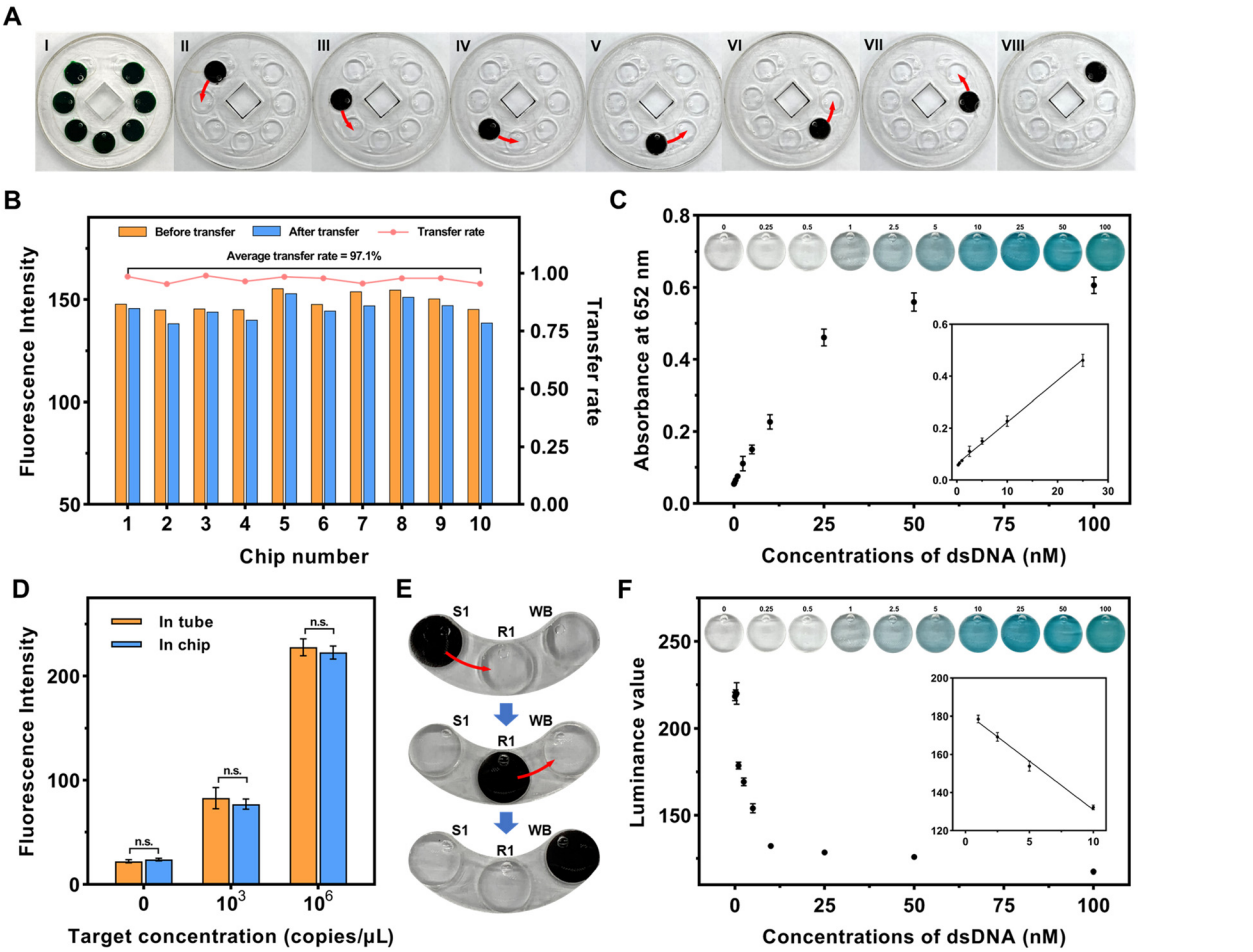

Fig. 2 Establishment and optimization of the detection system based on dCas12a in the up and down chip. (A) Characterization of the up and down chip. (I) Investigation of oil/water phase separation and stability. A green aqueous solution filled the circular chambers, while a colorless mineral oil filled the arched chamber above them. (II–VIII) Migration of dCas12a-modified MBs in each aqueous chamber inside the chip and no significant retention was observed. (B) The total migration efficiency of MBs inside the chip measured in ten parallel chips. (C) Response of the absorbance at 652 nm *vs.* the concentrations of target dsDNA in the detection system based on dCas12a out of the up and down chip (with three technical replicates). The inset showed the linear range of this response. (D) Comparison of RT-RAA amplification efficiency inside and outside the chip (with three technical replicates. n.s.: no significance in Student's *t*-test). (E) Migration of MBs during the S_1-R_1-WB process with the introduction of RT-RAA reagents in R_1 and no significant retention was observed. (F) Response of the luminance value *vs.* the concentrations of target dsDNA in the detection system based on dCas12a in the up and down chip (with three technical replicates). The inset showed the linear range of this response.

enhanced green fluorescent protein (EGFP)-modified MBs. After different migration times, the remaining fluorescence intensity (λ_{Ex}: 490 nm, λ_{Em}: 510 nm) in the chamber was measured, and it is found in Fig. S2A† that the increase in surfactant concentration improved the migration efficiency of MBs. Because an excessively high concentration of surfactant may potentially affect the reactions, a moderate concentration of 0.75% surfactant was chosen for subsequent practical use. Meanwhile, the thickness of layers below 1 mm was beneficial to the migration efficiency of MBs; thus 0.5 mm was ultimately chosen (Fig. S2B†). Under these optimized conditions, the complete migration process of MBs in the chip is shown in Fig. 2A (II–VIII), and no obvious retention of MBs was observed. Subsequent parallel testing of 10 chips revealed that the overall migration efficiency of MBs was 97.1% and acceptable (Fig. 2B).

Establishment of the recognition system based on dCas12a

Based on previous literature, the mutation site (E925A) of dCas12a occurred in the RuvC domain of the NUC lobe (Fig. S3†), which was directly related to DNA cleavage ability.[6,26] According to Fig. S4A,† dCas12a was solubly expressed and purified from the prokaryotic expression system. A comparison between dCas12a and wild-type LbCas12a was conducted using a conventional CRISPR fluorescence reporting assay (the protocol is shown in the ESI†). The results demonstrated that neither dsDNA nor ssDNA can activate the *trans*-cleavage activity of dCas12a (Fig. S4B†), while the specific binding capacity of dCas12a to target dsDNA mediated by crRNA was confirmed using native polyacrylamide gel electrophoresis. As shown in Fig. S4C,† a band of the complex with a higher molecular weight than that of unbound dsDNA was visible in the presence of

dCas12a–crRNA, while there was no apparent complex band for unmatched dsDNA. Therefore, dCas12a could firmly capture the target dsDNA fragments in the RT-RAA products without damage and could be adopted for the subsequent detection system.

Feasibility of the up and down chip for HIV-1 detection

The feasibility of the up and down chip-based detection platform was tested. As a reference, the biotin-labeled dsDNA was used as a mimic of the RT-RAA amplification product, and the entire reaction was completed in a 1.5 mL Eppendorf tube. As shown in Fig. S5,† this reaction produced a more obvious blue color and higher absorbance at 652 nm with the increase of dsDNA concentration, and as low as 0.98 nM dsDNA could be directly distinguished by the naked eye without nucleic acid amplification, while the sensitivity could be improved to 0.49 nM with the aid of a plate reader. When the up and down chip was applied (Fig. 2C), the color change and absorbance generated in the R_3 chamber were positively correlated with the concentration of dsDNA within a certain range, and the sensitivity of visible detection was also comparable to that of the reference.

In addition, the amplification efficiency of RT-RAA within or out of the chip was also characterized at the same temperature of 42 °C and reaction time. When equal amounts of products were introduced into the CRISPR fluorescence reporting assay (Fig. 2D), no significant differences were observed in both fluorescence signals and backgrounds between the two reactions. Since the RT-RAA reaction mixture was highly viscous due to the high concentration of PEG, the migration of MBs during the S_1-R_1-WB process should be evaluated. As shown in Fig. 2E, no obvious retention of MBs was observed during the migration after the RT-RAA reaction. The above results indicated that nucleic acid detection based on dCas12a could be feasibly performed inside the up and down chip.

Feasibility of the signal readout system based on smartphone application

To bypass the dependence on large instruments for signal readout, an image recognition app from a smartphone was adopted to convert the monocolor change in R_3 into image brightness or other parameter change. The basic mode of signal transduction is shown in Fig. S6A,† in which the RGB values of R_3 were extracted and calculated according to Formula (1), so the corresponding brightness was obtained and reflected the concentration of the target nucleic acid fragment. Initially, gold nanoparticles (AuNPs) with stable and characteristic wine-red color were used for validation. As shown in Fig. S6B–F,† different concentrations of AuNPs presented varying shades of color. The RGB values were measured by a smartphone app (Fig. S7†) and converted to the luminance values (LV values) by Formula (1).[27,28] The results showed that the LV value was correlated with the characteristic absorption peak at 520 nm. Therefore, it was feasible to perform the signal transduction and output based on the above mode.

$$\text{Luminance value (LV)} = 0.30R + 0.59G + 0.11B \quad (1)$$

Following the same principle, the detection results from the R_3 chamber in the up and down chip (Fig. 2C) were also converted into the LV values (Fig. 2F), which were negatively correlated with the concentration of target dsDNA within a certain range. Consequently, the application of this image recognition app could enable the semiquantitative output of the detection signal by a common smartphone.

Design and characterization of the portable heating box

In consideration of portability, a simple homemade constant-temperature box was developed (Fig. 3A). Using two types of power suppliers (a household socket with a transformer and a lithium battery), the heating performance of the device was tested. For either supplier (Fig. 3B), the MCH heater could reach around 50 °C within 10 min and maintained for at least 45 min. The temperature of the chambers inside the chip reached around 40 °C within 20 min and remained stable for 40 min, which were relatively lower than those of the MCH. Considering the simplicity and portability of the device, the battery was used as the power supplier in the subsequent work. Further tests on seven chambers of five chips showed that the temperatures inside these chambers ranged from 37.8 to 39.9 °C after a 20-min preheating. Then the detection response of the system to 10 nM mimic target was examined at different temperatures. As shown in Fig. 3D and E, the ΔLV value of the R_3 chamber, which was the difference between the LV values from the blank group (20 μL ddH_2O as the sample) and the experimental group, remained relatively stable within the temperature range of 35–40 °C. Therefore, the developed portable heating box was suitable for practical application in the detection system.

Detection sensitivity analysis

After the establishment of the up and down chip-based detection system, its performance was evaluated using HIV-1 as the model target. By comparing with the Los Alamos National Laboratory database (as shown in Fig. S9†) and analyzing, a relatively conserved detection site was identified on the *pol* gene of the standard strain. However, the common TTTV PAM site for recognition of dCas12a was not observed in this fragment, so a mismatch design of RT-RAA primers was adopted based on previous work[9] to form an artificial PAM site (the feasibility of this strategy is shown in Fig. S10†). Next, the impacts of two common sample pretreatment methods, including the heat lysis and the MB extraction, on the detection sensitivity were investigated. As shown in Fig. 4A and B, the HIV-1 concentration for visual identification was at least 1000 and 250 CPs per mL in these two methods, respectively. According to the National

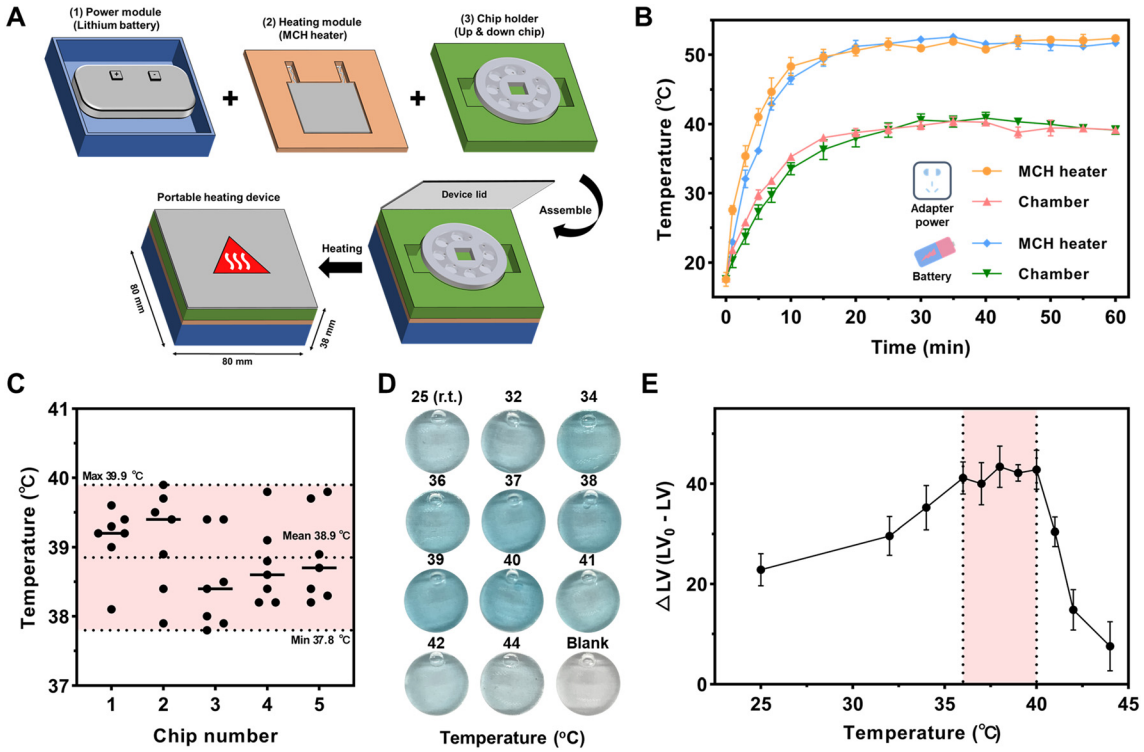

Fig. 3 Design and characterization of the portable heating box. (A) Basic modules and assembly method of the heating box. (B) Monitoring the temperature of the MCH and the up and down chip with different power suppliers over time. (C) Temperature measurements of all chambers from five chips after a 20-min preheating of the device. (D) Response of the color changes *vs.* 10 nM mimic target at different temperatures. (E) Response of ΔLV (the difference between the LV values of the blank group and the experimental group) *vs.* 10 nM mimic target at different temperatures.

Guideline for Detection of HIV/AIDS (2020), the cut-off line for preliminary diagnosis of HIV-1 is 5000 CPs per mL; thus the detection sensitivity of either method could fulfill clinical testing requirements. Considering the detection sensitivity, the main influencing difference between the two methods was the template volume used for the RT-RAA reaction. Since the maximum template volume in the chip was 20 μL, the MB extraction could perform within this range, while the heat lysis without a pre-enrichment effect required a much larger sample volume, so the MB extraction method was adopted in the subsequent process.

Universality analysis in variant detection

HIV-1 has numerous variants; the most common ones include the B subtype and the circulating recombinant form (CRF) 01_AE, 07_BC, and 08_BC, *etc.* (Fig. S9†). Therefore, 16 variants listed in Fig. 5A were selected to investigate the

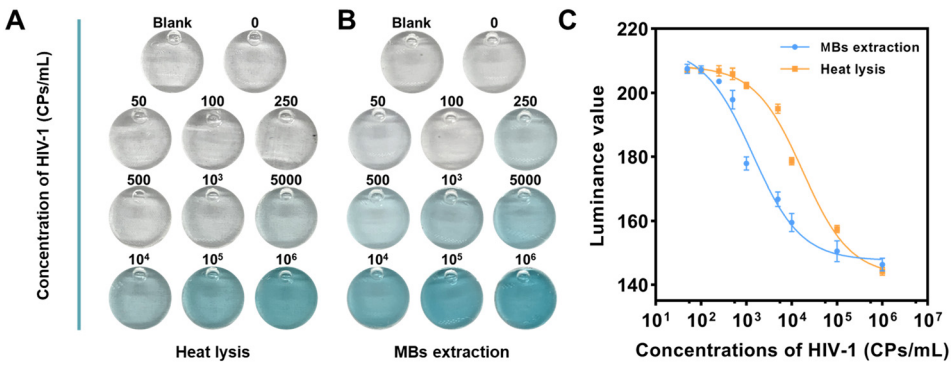

Fig. 4 Investigation of the sensitivity of the up and down chip for HIV-1 detection. (A) Response of the color change *vs.* different concentrations of HIV-1 pseudovirus by using the up and down chip combined with heat lysis. (B) Response of the color changes *vs.* different concentrations of HIV-1 pseudovirus by using the up and down chip combined with MBs extraction. (C) Response of the luminance values *vs.* different concentrations of HIV-1 pseudovirus by using the up and down chip combined with two kinds of pretreatment methods (with three technical replicates).

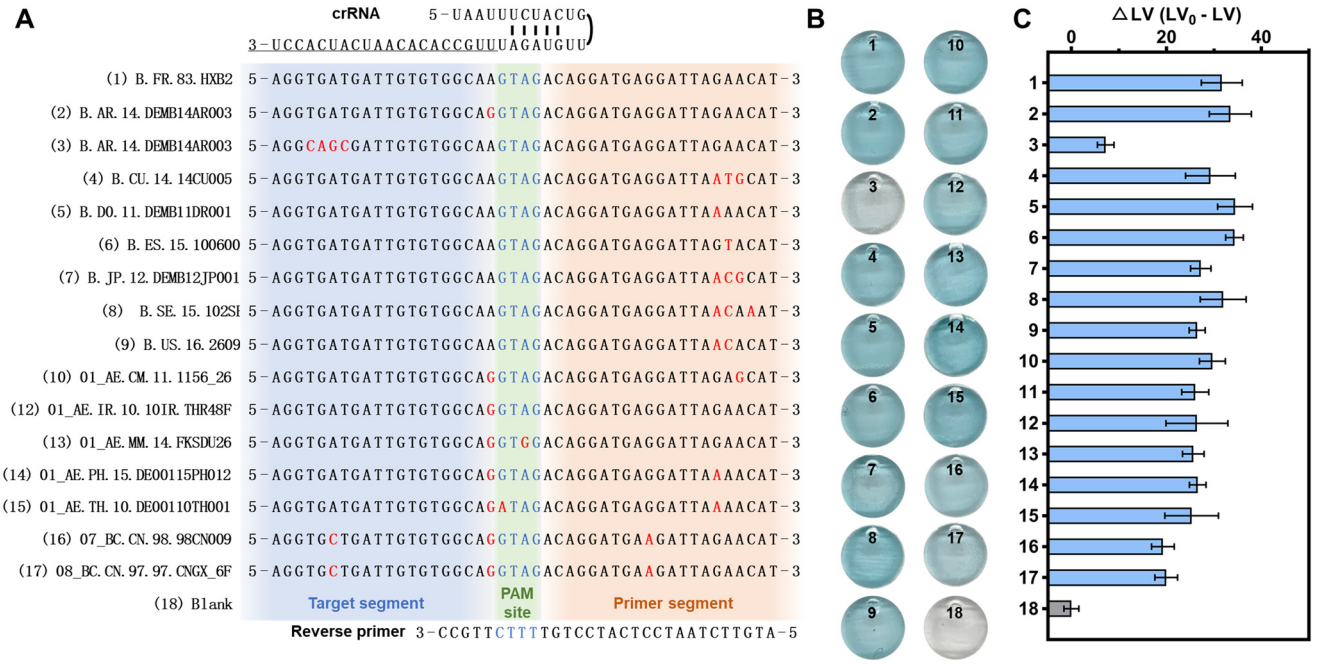

Fig. 5 Investigation of the universality of the up and down chip for HIV-1 variant detection. (A) Sequence alignment of common HIV-1 variants (no. 2–17) and the standard strain (no. 1) as well as the mismatches with crRNA and RT-RAA-RP-PAM. (B) Response of the color changes *vs.* 5000 CPs per mL mimic targets from HIV-1 variants or the standard strain by using the up and down chip. (C) Response of ΔLV *vs.* 5000 CPs per mL mimic targets from HIV-1 variants or the standard strain by using the up and down chip (with three technical replicates).

universality of the detection system at 5000 CPs per mL (Fig. 5B and C). Compared with the standard strain, the chip could effectively recognize the variants (no. 2, 4–15) with the base substitutions in the primer segment, the PAM site, or the upstream region of the target segment (1–5 bases), and the corresponding color changes were observed as well. When mutations occurred in the key region of the target segment, which could cause significant changes in the binding ability of dCas12a, the color changes induced by these variants (no. 3, 16–17) were attenuated in different levels, but still recognizable to the naked eye. The potential effect of the target sequence on the detection sensitivity was further validated using the CRISPR fluorescence reporting assay (Fig. S11†). The results suggested that the continuous mismatches between the crRNA and the target segment, especially in the seed region near the PAM site, significantly reduced the binding ability of Cas12a and slowed down its *trans*-cleavage rate, which was consistent with the results shown in Fig. 5 and the reported conclusions.[7]

Characterization of the potential for clinical detection

Since HIV-1 infection often leads to opportunistic infections (OIs), the specificity of the detection system was evaluated on different samples, including common OI pathogens *Candida albicans*, *Aspergillus fumigatus*, *Cryptococcus neoformans*, *Pseudomonas aeruginosa*, *Staphylococcus aureus*, and HIV-2 (pseudovirus) with about 55% gene similarity to HIV-1. As shown in Fig. 6A, no obvious color changes were observed in OI pathogens and HIV-2; even their concentrations were ten times higher than that of HIV-1 (5000 CPs per mL), and their corresponding ΔLV values also showed no significant difference compared to the blank. Therefore the up and down chip presented a clear response and good specificity to HIV-1.

The anti-interference ability of the up and down chip was also investigated by addressing the actual clinical samples. Specifically, 10^4, 5000, 10^3, and 0 copies per milliliter of HIV-1 pseudovirus were spiked into plasma, saliva, and urine from healthy volunteers or 1× PBS buffer and were tested, respectively. As shown in Fig. 6B and C, no significant difference in the color change and ΔLV value was observed among different types of samples with the same concentration of HIV-1 pseudovirus. Consequently, the up and down chip was capable of dealing with complex matrices in clinical samples because of the purifying effects of the MB extraction method.

Subsequently, the detection accuracy of the chip was investigated using the most common plasma samples. Similarly, 28 HIV-1 positive samples (10^6–250 CPs per mL) and 28 negative samples (0 CPs per mL) were obtained by spiking, and they were individually tested using the chip. Fig. 6D and Table S4† exhibit the detection results extracted from the R_3 chambers and the receiver operating characteristic curve (ROC) was constructed (Fig. 6E). These results revealed that the up and down chip showed good diagnostic accuracy with an area under the curve (AUC) of

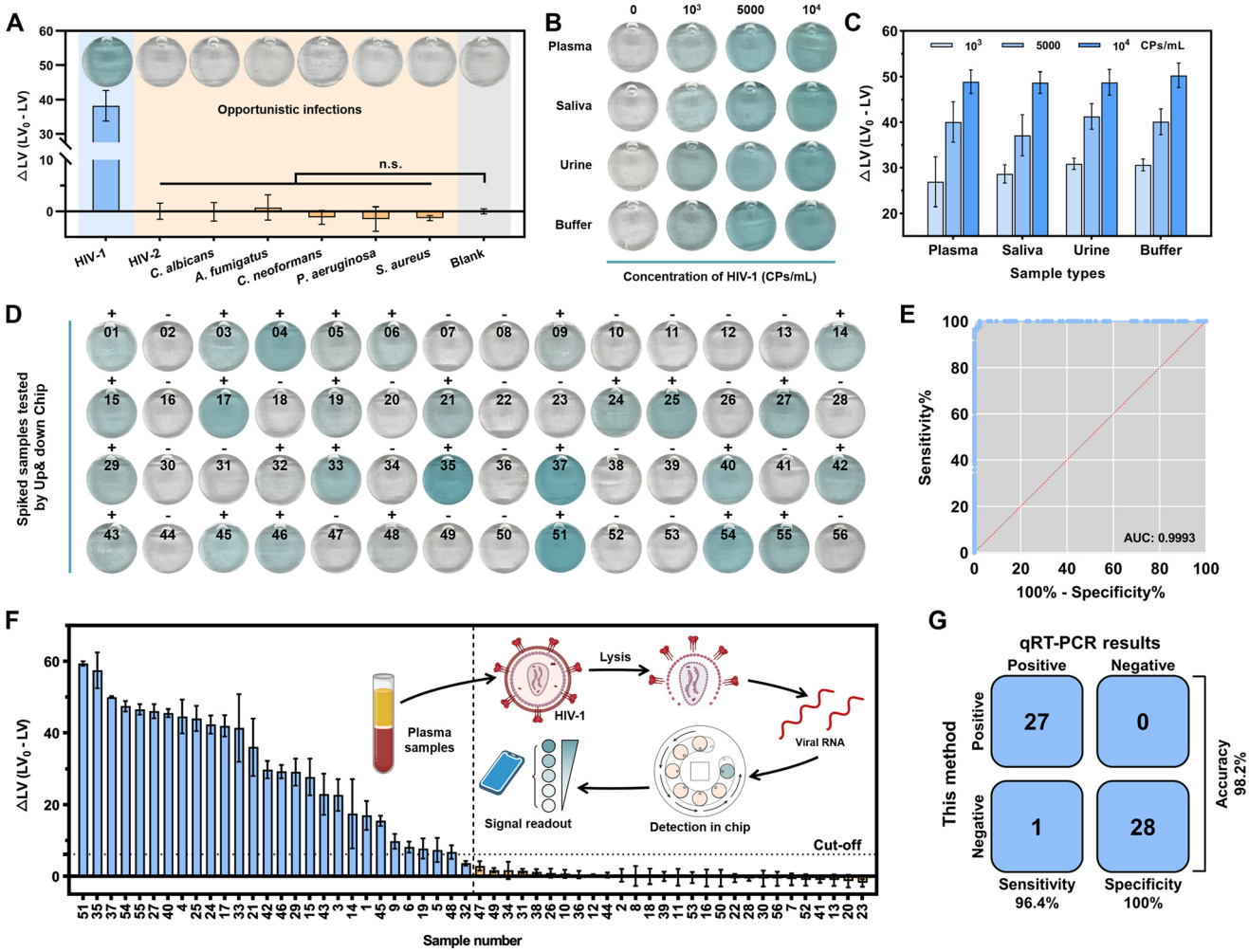

Fig. 6 Characterization of the potential for clinical detection. (A) Specificity characterization of HIV-1 detection by the up and down chip. *C. albicans*, *A. fumigatus*, *C. neoformans*, *P. aeruginosa*, *S. aureus*, and HIV-2 (pseudovirus) at 50 000 CPs per mL were used as negative controls which was 10 times the concentration of HIV-1 (with three technical replicates. n.s.: no significance in Student's *t*-test). (B) Response of the color changes *vs.* different concentrations of HIV-1 pseudovirus in different types of spiked sample (plasma, saliva, urine, and 1× PBS buffer) by using the up and down chip. (C) Response of ΔLV *vs.* different concentrations of HIV-1 pseudovirus in different types of spiked sample (plasma, saliva, urine, and 1× PBS buffer) by using the up and down chip (with three technical replicates). (D) Response of the color changes *vs.* spiked HIV-1 samples, including 28 positive and 28 negative ones. (E) Receiver operating characteristic curve of the up and down chip for HIV-1 detection. The area under the curve (AUC) was 0.9993 if each parallel test is considered as an independent measurement. (F) Response of ΔLV *vs.* spiked HIV-1 samples, including 28 positive and 28 negative ones. The average value of ΔLV in the negative control plus three times the standard deviation was set as the cut-off line for diagnosis. (G) Sensitivity, specificity, and overall accuracy analysis of the up and down chip compared to qRT-PCR.

0.9993. When the average value of the negative control signal plus the three times standard deviation was set as the cut-off line for diagnosis (Fig. 6F), only one false negative result was observed in sample 32, whose spiked concentration was 250 CPs per mL and close to the detection limit of the chip, but still much lower than the objective concentration for HIV-1 screening (5000 CPs per mL). These results were also compared with those from qRT-PCR (Fig. S12 and Table S4†), the "gold standard" of clinical nucleic acid detection. Based on this criterion, the sensitivity, specificity, and overall accuracy of the chip detection were 96.4%, 100%, and 98.2%, respectively. It can be observed in Table S5† that the costs of the up and down chip assay and qRT-PCR were similar in terms of reagents and consumables. Moreover, a significant advantage was also demonstrated with the up and down chip, especially in the absence of professional instruments.

Compared to other commonly used techniques in HIV-1 clinical diagnosis, such as immunoassays including enzyme-linked immunoassay and chemiluminescence immunoassay, the up and down chip, as a nucleic acid-based detection method, is expected to offer better sensitivity and specificity. This implies a shorter detection window period, which holds significant importance for early diagnosis and improving survival rates. Additionally, the flexibility of the CRISPR system and the universality of

this chip may confer advantages in addressing viral mutations.

Conclusion

A magnetofluid-integrated biosensor-based detection device named "up and down chip" was established for visual point-of-care testing of nucleic acid. The device combined RT-RAA technology for nucleic acid amplification, dCas12a-modified MBs for specific recognition of target nucleic acid, and HRP–TMB chromogenic reaction for signal output. The device used a magnetically driven process similar to ELISA for convenient detection of target nucleic acid on a simple microfluidic chip, achieving a "sample-in, result-out" testing mode and preventing aerosol contamination during sample transfer. It included a homemade heating box for temperature control during the reaction and enabled result reading using the naked eye or a smartphone app, eliminating the dependence on professional instruments. By clinical simulation targeting HIV-1, the device showed a high sensitivity for detecting as low as 250 CPs per mL target fragments within 100 min, and it also presented excellent specificity resistant to background interference and good accuracy for 56 spiked samples. However, for large-scale clinical applications, the detection operation mode and throughput still need further improvement, such as developing a portable device to automate the loading of reagents and the driving of MBs and incorporating array-based channels or chips to increase the detection throughput.

Author contributions

Di Huang: investigation, formal analysis, methodology, writing – original draft. Yekai Zhao: investigation, formal analysis, validation. Mengjun Fang: formal analysis, investigation, methodology. Peijie Shen: investigation, methodology. Hu Xu: investigation, resources. Yichen He: investigation, resources. Shengfu Chen: investigation, validation. Zhenjun Si: validation, resources. Zhinan Xu: supervision, project administration, funding acquisition, writing – review & editing.

Conflicts of interest

The authors declare no conflict of interest.

Acknowledgements

This work was financially supported by the National Key Research and Development Program of China (2021YFC2103200) and the Agricultural and Social Development Research Project of Hangzhou (202204B01).

References

1 Z. Li, X. Xu, D. Wang and X. Jiang, *TrAC, Trends Anal. Chem.*, 2023, **158**, 116871.
2 H. M. Yoo, I.-H. Kim and S. Kim, *Int. J. Mol. Sci.*, 2021, **22**, 6150.
3 F. X. Liu, J. Q. Cui, Z. Wu and S. Yao, *Lab Chip*, 2023, **23**, 1467–1492.
4 Y. Tang, L. Gao, W. Feng, C. Guo, Q. Yang, F. Li and X. C. Le, *Chem. Soc. Rev.*, 2021, **50**, 11844–11869.
5 T. Yamano, H. Nishimasu, B. Zetsche, H. Hirano, I. M. Slaymaker, Y. Li, I. Fedorova, T. Nakane, K. S. Makarova, E. V. Koonin, R. Ishitani, F. Zhang and O. Nureki, *Cell*, 2016, **165**, 949–962.
6 D. C. Swarts and M. Jinek, *Mol. Cell*, 2019, **73**, 589–600.
7 J. S. Chen, E. Ma, L. B. Harrington, M. D. Costa, X. Tian, J. M. Palefsky and J. A. Doudna, *Science*, 2018, **360**, 436–439.
8 D. Huang, J. Qian, Z. Shi, J. Zhao, M. Fang and Z. Xu, *ACS Synth. Biol.*, 2020, **9**, 3114–3123.
9 D. Huang, D. Ni, M. Fang, Z. Shi and Z. Xu, *Anal. Chem.*, 2021, **93**, 16965–16973.
10 D. Huang, Z. Shi, J. Qian, K. Bi, M. Fang and Z. Xu, *Biotechnol. Bioeng.*, 2021, **118**, 1587–1596.
11 M. Sohail, S. Xie, X. Zhang and B. Li, *Anal. Chim. Acta*, 2022, **1205**, 339541.
12 R. Nouri, M. Dong, A. J. Politza and W. Guan, *ACS Sens.*, 2022, **7**, 900–911.
13 H. Wu, Y. Chen, Y. Shi, L. Wang, M. Zhang, J. Wu and H. Chen, *Biosens. Bioelectron.*, 2021, **178**, 113001.
14 W. Feng, H. Peng, J. Xu, Y. Liu, K. Pabbaraju, G. Tipples, M. A. Joyce, H. A. Saffran, D. L. Tyrrell, S. Babiuk, H. Zhang and X. C. Le, *Anal. Chem.*, 2021, **93**, 12808–12816.
15 Y. Chen, Y. Shi, Y. Chen, Z. Yang, H. Wu, Z. Zhou, J. Li, J. Ping, L. He, H. Shen, Z. Chen, J. Wu, Y. Yu, Y. Zhang and H. Chen, *Biosens. Bioelectron.*, 2020, **169**, 112642.
16 X. Xu, L. Lin, J. Yang, W. Qian, R. Su, X. Guo, L. Cai, Z. Zhao, J. Song and C. Yang, *Nano Today*, 2022, **46**, 101596.
17 J. Yin, Z. Zou, F. Yin, H. Liang, Z. Hu, W. Fang, S. Lv, T. Zhang, B. Wang and Y. Mu, *ACS Nano*, 2020, **14**, 10385–10393.
18 Y. Liu, H. Shen, X. Yang, S. Kang, L. Cai, T. Tian, R. Su, C. Yang and Z. Zhu, *TrAC, Trends Anal. Chem.*, 2023, **158**, 116894.
19 Z. Li, X. Ding, K. Yin, L. Avery, E. Ballesteros and C. Liu, *Biosens. Bioelectron.*, 2022, **199**, 113865.
20 Y. Chen, Y. Mei, X. Zhao and X. Jiang, *Anal. Chem.*, 2020, **92**, 14846–14852.
21 M. Serra, E. Gontran, I. Hajji, L. Malaquin, J. L. Viovy, S. Descroix and D. Ferraro, *Adv. Mater. Technol.*, 2020, **5**, 1901088.
22 H. Shen, X. Chen, L. Zeng, X. Xu, Y. Tao, S. Kang, Y. Lu, M. Lian, C. Yang and Z. Zhu, *Anal. Chem.*, 2022, **94**, 8458–8465.
23 Z. Wu, C. Wang, B. Liu, C. Liang, J. Lu, J. Li, X. Tang, C. Li and T. Li, *ACS Sens.*, 2022, **7**, 1985–1995.
24 K. Fan, J. Zeng, C. Yang, G. Wang, K. Lian, X. Zhou, Y. Deng and G. Liu, *ACS Sens.*, 2022, **7**, 2049–2057.

25 T. Hu, X. Ke, W. Li, Y. Lin, A. Liang, Y. Ou and C. Chen, *Adv. Sci.*, 2022, **10**, 2204689.
26 K. Ciurkot, T. E. Gorochowski, J. A. Roubos and R. Verwaal, *Nucleic Acids Res.*, 2021, **49**, 7775–7790.
27 S. Chen, S.-N. Yun, Y. Liu, R. Yu, Q. Tu, J. Wang and M.-S. Yuan, *Analyst*, 2022, **147**, 3258–3265.
28 S. Wei, J. Li, J. He, W. Zhao, F. Wang, X. Song, K. Xu, J. Wang and C. Zhao, *Microchim. Acta*, 2020, **187**, 554.